ADVANCES IN PHYSICS, 1995, VOL. 44, NO. 2, 187–210

Anomalous normal-state properties of high-T_c superconductors: intrinsic properties of strongly correlated electron systems?

By TH. PRUSCHKE

Institut für Theoretische Physik, Universität Regensburg, 93040 Regensburg, Germany

M. JARRELL

Department of Physics, University of Cincinnati, Cincinnati, Ohio 45221, USA

and J. K. FREERICKS

Department of Physics, Georgetown University, Washington, DC 20057, USA

[Received 22 February 1995; accepted 31 July 1995]

Abstract

A systematic study of optical and transport properties of the Hubbard model, based on the Metzner–Vollhardt dynamical mean-field approximation, is reviewed. This model shows interesting anomalous properties that are, in our opinion, ubiquitous to single-band strongly correlated systems (for all spatial dimensions greater than one) and also compare qualitatively with many anomalous transport features of the high-T_c cuprates. This anomalous behaviour of the normal-state properties is traced to a 'collective single-band Kondo effect', in which a quasiparticle resonance forms at the Fermi level as the temperature is lowered, ultimately yielding a strongly renormalized Fermi liquid at zero temperature.

Contents

0001–8732/95 $25·00

1. Introduction and survey

The discovery of the high-T_c superconductors based on CuO compounds [1] has led to a large amount of theoretical work about the peculiar properties of these materials. While initial work concentrated on explaining the anomalous high transition temperatures and possible exotic mechanisms for the superconductivity, it became obvious that an understanding of the superconducting mechanism is linked to an understanding of the anomalous normal-state properties of these compounds (for reviews of relevant experiments see [2]). Most prominent among these are the linear (in T) resistivity, a linear (in T) nuclear magnetic resonance (NMR) relaxation rate of the Cu spins, a Hall coefficient which is positive and goes through a (roughly) doping-independent maximum and a Hall angle $\cot\Theta_H = \rho(T)/R_H(T)$ that grows like T^2 over a rather wide temperature region (figure 1 [3]). Furthermore, the optical conductivity shows a Drude peak with a width $1/\tau \sim T$ [4], consistent with the linear behaviour of the resistivity and a pronounced midinfrared peak at frequencies above the Drude peak (figure 2 [5]).

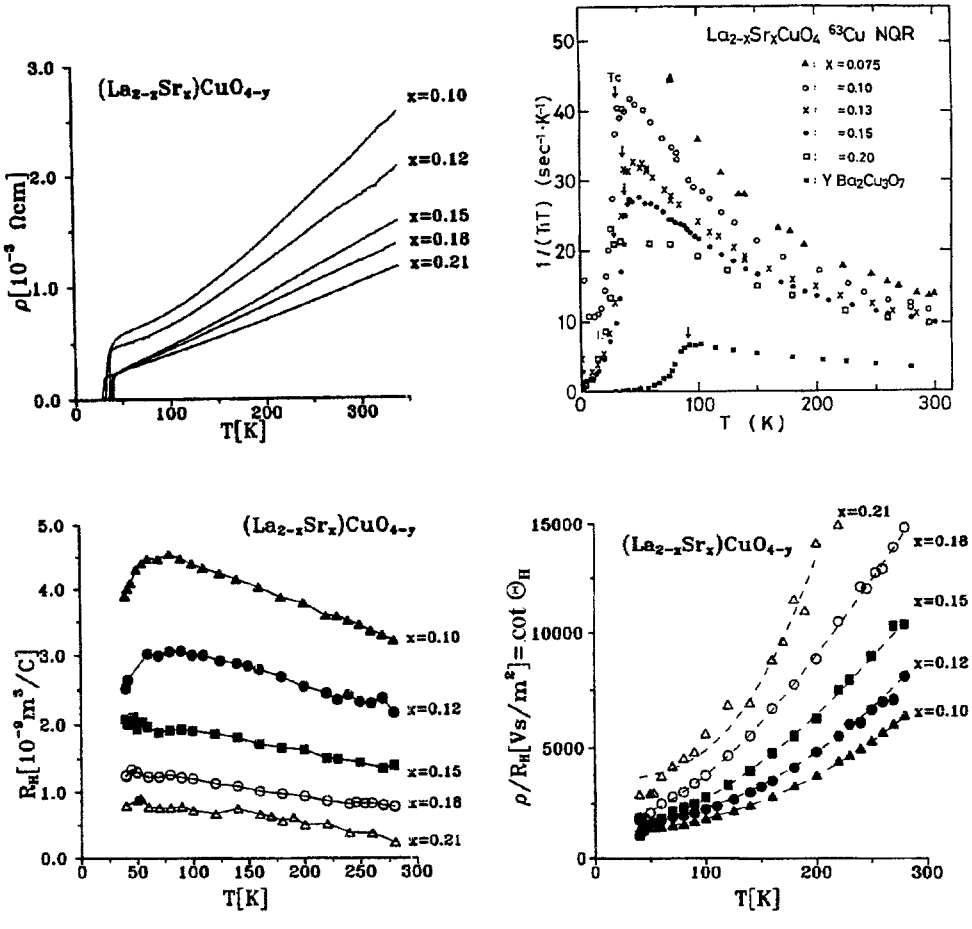

Figure 1. Typical experimental results for resistivity ρ, NMR relaxation rate T_1, Hall coefficient R_H and inverse mobility $1/\mu$ in high-T_c compounds (from [3]).

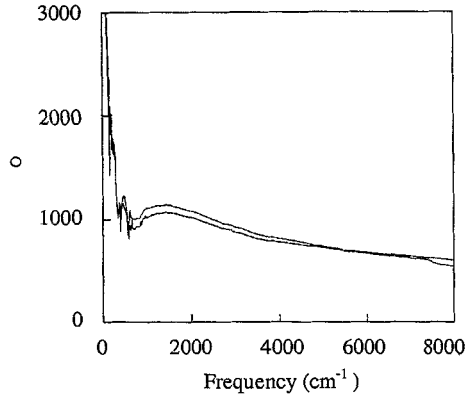

Figure 2. Experimental optical conductivity of $TlBa_2Ca_2Cu_3O_9$ (from [5]). Note the prominent midinfrared peak at about 1500 cm^{-1}.

Early on, it was argued [6] that most of these anomalous properties can be explained by two special features appearing simultaneously in these materials.

(1) They are strongly correlated, that is their (effective) local Coulomb interaction is comparable with or larger than the characteristic kinetic energy of the relevant carriers.
(2) They are highly anisotropic with the electrons confined to the CuO planes characteristic for these compounds.

This mixture of strong correlations and effective two-dimensional (2D) character is unusual and can only be found (apart from the cuprates and other perovskites) in some uranium-based heavy-fermion compounds such as UPt_3. The great interest in the high-temperature superconductors has led to a number of interesting new theories which, although based on the assumption of strongly correlated carriers, focused mainly on the 2D character of the CuO planes. Most prominent are the concept of resonating valence bonds due to Baskaran and Anderson [7], recent efforts by Solyom [8] and Anderson [9] to understand the electronic properties phenomenologically in terms of a Luttinger-liquid fixed-point (known from the theory of one-dimensional (1D) electron systems), the phenomenological marginal Fermi-liquid theory of Varma *et al.* [10], and the anyon concept emerging from a mapping of the 2D electron system onto a nonlinear σ model due to Lee and Nagaosa [11]. While the second and third ansatze have not been ruled out, both the first and the last are insufficient to account for the experimental data of these systems.

However, even in the theories of Anderson and of Varma *et al.* one needs additional assumptions about relaxation times [9] or dynamical quantities [10] to account consistently for *all* anomalies. Both theories also lack a thorough microscopic foundation. It is unclear how the special form of the single-particle self energy and the dynamical susceptibility (necessary for the marginal Fermi-liquid picture) will emerge. Even introducing a special three-body scattering vertex [12] does not resolve this difficulty, since it merely shifts the problem to another level. A foundation for Anderson's Luttinger-liquid picture is even less firm. The special feature of 1D systems, namely that the exchange of charge over a given site is strongly hindered by the Coulomb correlations, while the exchange of spin costs almost no energy [13] (which leads to the strict separation of spin and charge degrees of freedom), may already be

absent in two dimensions, since a physical electron may move 'around' any other via a path in the plane. Recent studies on the stability of the possible low-energy fixed points in interacting fermion models also suggest that it is the Fermi-liquid rather than the Luttinger-liquid fixed point that is stable in two dimensions (unless the small-momentum-transfer couplings become singular) [14].

There is another feature of strongly correlated systems that is usually ignored in dealing with the cuprates. From the experimental and theoretical investigation of heavy-fermion compounds it is known that the strong correlations themselves already lead to anomalous features in the magnetic and transport properties of metals. These systems are usually three dimensional (3D) in nature and, despite their complicated band structure [15], one can explain their physical properties qualitatively (and to some extent even quantitatively) by merely taking into account *one* strongly correlated localized band hybridizing with *one* uncorrelated conduction band [16]. This suggests that the prominent anomalous features of the heavy-fermion materials are intrinsic to the strong local correlations. Thus to understand unambiguously the origin of any anomalous behaviour in systems with strong electronic correlations, it is necessary to discriminate between those properties that are intrinsic and arise directly from the strong (local) electron–electron scattering, and those that are connected to the geometry of the underlying lattices, for example the 2D character of the Cu–O planes in the cuprates.

In previous publications [17, 18] we demonstrated that, even for the simplest model of strong local correlations, the single-band Hubbard model, interesting anomalous results for several different transport quantities occur which appear to be intrinsic properties of strongly correlated systems. This latter statement is motivated by the fact that our calculations use the Metzner–Vollhardt 'dynamical mean-field approximation' (for a review of the $d = \infty$ approach see [19]), which may be viewed as the fermionic equivalent of the standard non-local mean-field description of models for magnetism. As is well known, such a 'proper' mean-field description will in general reproduce the *intrinsic* features of the underlying model. Fluctuation corrections should affect only phase transitions and the quantitative values of temperature scales.

In this review we present a more detailed discussion of the transport properties of strongly correlated systems described by the Hubbard model in equation (1) (section 2). Special emphasis is placed on a thorough discussion of the variation in quantities with temperature and doping. We also try to make qualitative contact with recent experiments on optical and transport properties of the cuprates. The paper is organized as follows. In the next section an introduction into the underlying theory (the so-called dynamical mean-field theory) is given. We also give a brief account of how the transport properties are calculated. In section 3 the systematics for several quantities as functions of temperature and doping are presented and compared with experiment. A discussion and outlook in section 4 conclude the review.

2. Theoretical background

The model discussed in this contribution is the single-band Hubbard model [20]

$$H = \sum_{\mathbf{k}\sigma} \varepsilon_{\mathbf{k}} c^{\dagger}_{\mathbf{k}\sigma} c_{\mathbf{k}\sigma} + U \sum_{i} n_{i\uparrow} n_{i\downarrow}. \tag{1}$$

Our notation is the following: $c^{\dagger}_{\mathbf{k}\sigma}$ is the creation operator for an electron in a Bloch state with wave-vector $\mathbf{k}$ and z component of spin σ, and $n_{i\sigma}$ is the electron number operator for electrons localized at lattice site i with spin σ (i.e. the number operator for electrons in Wannier orbitals centred at lattice site i). For simplicity we restrict ourselves to a

simple hypercubic lattice (in d dimensions) with lattice constant a and nearest-neighbour transfer t, that is $\varepsilon_{\mathbf{k}} = -2t\Sigma_{i=1}^{d}\cos(k_i a)$; U denotes the local Coulomb repulsion. The energy scale is set by $4dt^2 =: t^{*2}$ (this is the required scaling for non-trivial results as $d \to \infty$) and the quantity t^* is thus an appropriate unit for the energy. For the cuprates, the width of the lower Cu band is often taken to be about 0·5 eV. If this corresponds to the lower Hubbard band, with a width of about $2t^*$ (cf. section 3.1), then $t^* \approx 0{\cdot}25$ eV.

The Hubbard model is perhaps the simplest model of a correlated electronic system, since it consists of a single band of delocalized electrons subject to a *local* Coulomb interaction. It is easier therefore to discriminate between intrinsic effects of the correlations (induced by the Coulomb interaction) from band-structure effects. Obviously, a more realistic description of a condensed-matter system must take into account the existence of more than one band, hybridizations between different bands, and also additional local and long-range Coulomb interactions. However, these more realistic models may be mapped onto the Hubbard model (1) when excitations into these other bands occur only virtually, leading to renormalized values for, for example $\varepsilon_{\mathbf{k}}$ [21]. Since the purpose of the present contribution is to identify effects intrinsic to the local correlations, these other interactions may be neglected.

Models of interacting electrons on a lattice are difficult to solve because they include both *local* and *non-local* parts in the Hamiltonian. The fundamental quantum-mechanical principle of complementarity implies that one cannot expect to describe such a system by either purely localized or purely delocalized states. Approximations starting from either side (i.e. bandwidth/$U \ll 1$ or bandwidth/$U \gg 1$) are not generally applicable to the intermediate regime (bandwidth $\approx U$). To obtain sensible results for the Hubbard model in this intermediate regime, the Hamiltonian (1) is usually studied with exact diagonalization techniques [22] or quantum Monte Carlo (QMC) methods (for example [23]). Both methods share the problem that they can only be applied to comparatively small system sizes (about 20 sites in exact diagonalization and about 100 sites in QMC (for not too low temperatures)). This restriction seriously affects any attempt to determine low-energy low-temperature properties and makes the calculation of dynamical quantities and transport properties difficult. An ansatz is therefore needed to calculate different physical quantities of strongly correlated systems that firstly maintains the important local correlations and secondly allows calculations to be performed in the thermodynamic limit.

Such a method was proposed by Metzner and Vollhardt [24] and Müller-Hartmann [25] who observed that the renormalizations due to local two-particle interactions like the Hubbard U become purely local as the coordination number of the lattice increases. More precisely, the irreducible single-particle self-energy $\Sigma_{\mathbf{k}}(z)$ and the irreducible two-particle self-energy $\Gamma_{\mathbf{k},\mathbf{k}+\mathbf{q}}(z, z')$ both become independent of momentum for large coordination numbers ($2d \to \infty$) [25, 26]:

$$\lim_{d\to\infty}[\Sigma_{\mathbf{k}}(z)] = \Sigma(z),$$
$$\lim_{d\to\infty}[\Gamma_{\mathbf{k},\mathbf{k}+\mathbf{q}}(z, z')] = \Gamma(z, z'). \tag{2}$$

One can use standard techniques of field theory to show that the second relation in equation (2) is a necessary consequence of the first for *all* two-particle self-energies [26]. A further consequence of the first relation is that the solution of the Hubbard model may be mapped onto the solution of a local correlated system coupled to an effective bath that is self-consistently determined by the following five-step process [26–31].

(1) Choose a suitable starting guess for the local self-energy $\Sigma(z)$.
(2) Calculate the local single-particle Green function from its Fourier transform:

$$G_{ii}(z) = \frac{1}{N} \sum_{\mathbf{k}} \frac{1}{[G_{\mathbf{k}}^{(0)}(z)]^{-1} - \Sigma(z)}, \tag{3}$$

with $G_{\mathbf{k}}^{(0)} := 1/(z + \mu - \varepsilon_{\mathbf{k}})$ the *non-interacting* momentum-dependent Green function.
(3) Obtain the effective medium, denoted by $\mathcal{G}(z)$, by subtracting off the local correlations from the Coulomb interaction at site i:

$$[\mathcal{G}(z)]^{-1} := (G_{ii})^{-1} + \Sigma(z). \tag{4}$$

(4) Solve the local impurity problem defined by the effective medium $\mathcal{G}(z)$ and the local Coulomb interaction $Un_{i\uparrow}n_{i\downarrow}$ at site i (via an exact quantum Monte Carlo algorithm, or an approximate algorithm based upon a diagrammatic analysis) to obtain a new local single-particle Green function $\tilde{G}(z)$.
(5) Obtain a new self-energy via $\Sigma(z) = [\tilde{G}(z)]^{-1} - [\mathcal{G}(z)]^{-1}$ and repeat steps (2)–(3) until the local Green functions are identical between two successive iterations ($G_{ii}(z) = G(z)$).

This mapping onto a local problem coupled to an effective bath is reminiscent of the standard mean-field description of spin systems. As is well known, such a theory emerges systematically from the same limit of large coordination number [32]. One major difference between electronic models and spin models is that in the former the Coulomb interaction introduces a non-trivial local dynamic that is preserved in the mean-field approach. The molecular field for the electronic mean-field theory is not a constant number but is instead a function of the energy, and hence the name 'dynamical mean-field theory'. These local electronic mean-field theories have a rich history, dating back to the Migdal–Eliashberg [33] theory of superconductivity; Metzner and Vollhardt [24] were the first to realize that these mean-field theories become exact solutions in the limit of infinite dimensions.†

Although the solution of the effective local system is still a highly non-trivial matter, it has the great advantage that one is able to work directly in the thermodynamic limit. Note that the lattice structure has not been completely eliminated from the problem. It enters indirectly via the free density of states (DOS), when momentum summations are converted to energy integrals, and it enters in the evaluation of susceptibilities, which still maintain a (weak) momentum dependence.

Three methods have proven to be most successful in solving the remaining local problem: a QMC scheme based on the work of Hirsch and Fye [34], (see also [30, 35]), a perturbational method known as the non-crossing approximation (NCA) [36] and the so-called iterated perturbation theory based on low-order expansion of $\Sigma(z)$ in U [31, 37]. The latter is, however, strictly limited to the case $\langle n \rangle = 1$ [38] and thus of no use for our purpose. The remaining two methods have of course also both their merits and disadvantages and may be viewed as complementary to each other, providing a means of accessing many different quantities of interest. A more detailed discussion of the limitations of both approaches can be found in our earlier publications [17, 39].

† The Migdal–Eliashberg dynamical mean-field theory becomes exact only in the limit of small phonon frequency. If the phonon frequency is large enough, vertex corrections must be included in the dynamical mean-field theory.

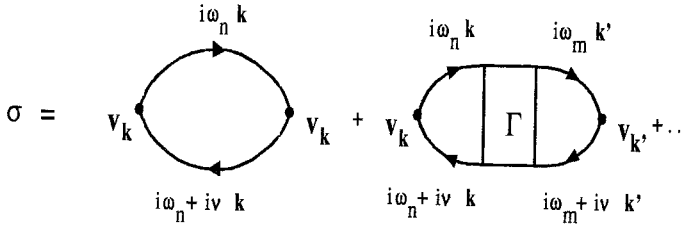

Figure 3. Diagrammatic representation of the first two contributions to the conductivity. The second diagram contains a *full* particle–hole vertex insertion. The latter is momentum independent, that is the **k** sums on both sides can be performed independently. Since the current vertex and the single-particle Green functions are of different parities (with respect to their **k** dependence), the second and all higher-order diagrams identically vanish.

Knowledge of the single-particle self-energy and the *local* two-particle vertex functions (which can also be determined from the same local problem) enables one to calculate physical quantities. As an illustration of this, an extended discussion of magnetism in the Hubbard model may be found in [39–41]. Other quantities of interest include the transport coefficients, the optical conductivity, the thermopower and the Hall coefficient. For example, the conductivity can be calculated exactly in the dynamical mean-field theory by the following procedure: figure 3 shows the leading diagrams in the expansion of the conductivity. As was discussed earlier, the particle–hole vertex appearing in the second and all higher-order diagrams is momentum independent. This means that the **k** sums on the left and right end of all diagrams, except for the simple bubble, may be performed independently. Since the current operator contains the **k** gradient of the kinetic energy, and the Green functions are **k** dependent only through $\varepsilon_{\mathbf{k}}$, these sums identically vanish. Thus the conductivity is given by the simple bubble only [17, 42, 43]. The evaluation of the bubble leads to

$$\sigma_{xx}(\omega) = \frac{\pi e^2}{2\hbar a}\int_{-\infty}^{\infty} \mathrm{d}\varepsilon \frac{f(\varepsilon) - f(\varepsilon+\omega)}{\omega} \frac{1}{N}\sum_{\mathbf{k}\sigma}\left(\frac{\partial \varepsilon_{\mathbf{k}}}{\partial k_x}\right)^2 A_{\mathbf{k}}(\varepsilon)A_{\mathbf{k}}(\varepsilon+\omega), \tag{5}$$

which reduces to

$$\sigma = \frac{e^2\pi}{2\hbar a}\int_{-\infty}^{\infty} \mathrm{d}\varepsilon \left(-\frac{\partial f(\varepsilon)}{\partial \varepsilon}\right) \frac{1}{N}\sum_{\mathbf{k}\sigma}\left(\frac{\partial \varepsilon_{\mathbf{k}}}{\partial k_x}\right)^2 [A_{\mathbf{k}}(\varepsilon)]^2, \tag{6}$$

for the dc conductivity, where a is the lattice constant, the spectral weight satisfies $A_{\mathbf{k}}(\omega) := -(1/\pi)\,\mathrm{Im}\,[G_{\mathbf{k}}(\omega)]$, and $f(\varepsilon) := 1/[1+\exp(\beta\varepsilon)]$ is the Fermi function. With $h/e^2 \approx 2{\cdot}6 \times 10^4\,\Omega$ the constants in front of equation (6) can be evaluated to yield $\sigma_0 \approx 10^{-3}$–$10^{-2}\,\mu\Omega^{-1}\,\mathrm{cm}^{-1}$.

The Drude weight D may be determined by extrapolation of the Matsubara-frequency current–current correlation function using the method proposed by Scalapino *et al.* [44]. This method sets a criterion to determine whether the ground state of a system is a metal, insulator or superconductor, by determining the asymptotic form of the current–current susceptibility in the x direction, $\Lambda_{xx}(\mathbf{q}, \mathrm{i}\nu_n)$ where $\nu_n = 2n\pi T$. Specifically, the Drude weight D is given by

$$D = \pi \lim_{T\to 0}[\langle -T_x\rangle e^2 - \Lambda_{xx}(\mathbf{q}=\mathbf{0}, 2\pi \mathrm{i}T)]. \tag{7}$$

Here, $\langle -T_x\rangle$ is the average kinetic energy per site, divided by the number of lattice dimensions.

Comparison of equations (5) with the standard expressions for transport coefficients [45] in the relaxation-time approximation shows that a variety of other transport coefficients may be calculated if one identifies

$$\tau_{xx}(\varepsilon) := \frac{1}{N}\sum_{\mathbf{k}\sigma}\left(\frac{\partial\varepsilon_{\mathbf{k}}}{\partial k_x}\right)^2 [A_{\mathbf{k}}(\varepsilon)]^2 \tag{8}$$

as the transport relaxation time. For example, the electronic contribution to the thermopower becomes [43, 45]

$$S = -\frac{k_B}{|e|}\beta\frac{L_{12}}{L_{11}}, \frac{k_B}{|e|} \approx 86\,\mu\mathrm{V\,K}^{-1}, \tag{9}$$

where L_{jk} are the standard transport integrals

$$L_{jk} = \int_{-\infty}^{\infty} \mathrm{d}\varepsilon \left(-\frac{\partial f(\varepsilon)}{\partial\varepsilon}\right) \tau^j(\varepsilon)\varepsilon^{k-1}. \tag{10}$$

It is known from studies of heavy-fermion systems that the relaxation-time approximation is sufficient to understand most zero-field properties. The Hall coefficient, however, is more sensitive to the approximations involved. Within the standard relaxation-time approximation the Hall coefficient satisfies

$$R_H = \frac{1}{-|e|}\frac{L_{11}}{L_{21}}. \tag{11}$$

Note that both L_{11} and L_{21} are positive, implying that the Hall coefficient is always negative and that the transport is electron like. Experiments, on the other hand, show that R_H can change sign in intermediate or low-temperature regions, and that the Hall coefficient is usually positive with an anomalous temperature dependence. An explanation for this theoretical deficiency was proposed by the phenomenological introduction of a 'skew-scattering' term [46]. However, a more refined treatment of the field-dependent conductivity can be performed [47]. The result is

$$\sigma_{xy}^H = \frac{2\pi^2|e|^3aB}{3\hbar^2}\int_{-\infty}^{\infty}\mathrm{d}\omega\left(\frac{\partial f(\omega)}{\partial\omega}\right)\frac{1}{N}\sum_{\mathbf{k}\sigma}\left(\frac{\partial\varepsilon_{\mathbf{k}}}{\partial k_x}\right)^2\frac{\partial^2\varepsilon_{\mathbf{k}}}{\partial k_y^2}[A_{\mathbf{k}}(\omega)]^3 \tag{12}$$

for the Hall conductivity. Here, B is the external magnetic field which points in the z direction. The constants in equation (12) can be rearranged according to $|e|^3aB/\hbar^2 = \sigma_0|e|a^2B/\hbar$ and $|e|a^2B/\hbar \approx 10^{-5}B$ $(1/T^{-1})$. Inserting the values for σ_0, we obtain $R_H = \sigma_{xy}/\sigma_{xx}^2 \approx 10^{-8}$–$10^{-9}B(m^3\,cT^{-1})$ as the unit for the Hall coefficient.

In the limit of large coordination number, and for a simple hypercubic lattice, the **k** sums in equations (8) and (12) can be further simplified to yield

$$\frac{1}{N}\sum_{\mathbf{k}\sigma}\left(\frac{\partial\varepsilon_{\mathbf{k}}}{\partial k_x}\right)^2 K(\varepsilon_{\mathbf{k}}) = \frac{2}{d}\int_{-\infty}^{\infty}\mathrm{d}\varepsilon N_0(\varepsilon)K(\varepsilon) \tag{13}$$

and

$$\frac{1}{N}\sum_{\mathbf{k}\sigma}\left(\frac{\partial\varepsilon_{\mathbf{k}}}{\partial k_x}\right)^2\frac{\partial^2\varepsilon_\kappa}{\partial k_y^2}K(\varepsilon_{\mathbf{k}}) = -\frac{1}{2d^2}\int_{-\infty}^{\infty}\mathrm{d}\varepsilon N_0(\varepsilon)\varepsilon K(\varepsilon), \tag{14}$$

with $K(\varepsilon_{\mathbf{k}})$ an arbitrary function depending on **k** through $\varepsilon_{\mathbf{k}}$ only, and $N_0(\varepsilon) := \exp[(\varepsilon/t^*)^2]/\pi(^{1/2}t^*)$ the non-interacting DOS.

Examination of equations (5) and (12)–(14) shows that the electronic conductivity is a $1/d$ effect and that the Hall effect enters to order $1/d^2$. In our calculations we

determine lowest-order quantities and calculate the *coefficient* of the $1/d$ term for σ_{xx} and the *coefficient* of the $1/d^2$ term for σ_{xy} (i.e. $\sigma_{xx} \to d\sigma_{xx}$ and $\sigma_{xy} \to d^2\sigma_{xy}$). Note, however, that $R_H = \sigma_{xy}/\sigma_{xx}^2$ enters to zeroth order and requires no rescaling!

Another important probe of the high-temperature superconductors involves NMR. The spin–lattice relaxation time T_1 characterizes the time needed to align the nuclear spins along the direction of the field. The local NMR relaxation rate satisfies

$$\frac{1}{T_1} = T \lim_{\omega \to 0} \left[\mathrm{Im} \left(\frac{\chi(\omega)}{\omega} \right) \right], \tag{15}$$

where $\chi(\omega)$ is the local dynamic spin susceptibility. Similarly, the spin-echo decay rate (or transverse nuclear relaxation rate) T_{2G} is another probe of the spin dynamics in the cuprates. T_{2G} satisfies a more complicated relation [48, 49]

$$\left(\frac{1}{T_{2G}} \right)^2 = C \left[\sum_{\mathbf{k}} F(\mathbf{k})^4 \chi(\mathbf{k})^2 - \left(\sum_{\mathbf{k}} F(\mathbf{k})^2 \chi(\mathbf{k}) \right)^2 \right], \tag{16}$$

with $\chi(\mathbf{k})$ the static momentum-dependent spin susceptibility, C an overall normalization factor and $F(\mathbf{k})$ the relevant form factor. The form factor involves the local site and the nearest-neighbour shell and assumes the form

$$F(\mathbf{k}) = 1 + \gamma \frac{2t}{U} \varepsilon_{\mathbf{k}}, \tag{17}$$

in infinite dimensions. Here, γ is a constant of order 1. The static susceptibility turns out to be a function of $-\varepsilon_{\mathbf{k}}/d^{1/2} =: X$ (in infinite dimensions), with $X = 0$ corresponding to the local susceptibility. The integrals over the form factors can be performed, to yield

$$\left(\frac{1}{T_{2G}} \right)^2 = \frac{C}{d} \left(2\gamma^2 \chi^2(X=0) - \frac{1}{2} \left| \frac{\mathrm{d}\chi(X)}{\mathrm{d}X} \right|_{X=0}^2 \right). \tag{18}$$

The inverse spin-echo decay rate is a $1/d^{1/2}$ effect in infinite dimensions, and it is effectively proportional to the local susceptibility, since the derivative of the momentum-dependent susceptibility with respect to X is an order of magnitude smaller than the susceptibility itself in the region of interest (see, for example, figure 1 of [40]). In fact, we neglect the derivative term when evaluating T_{2G} ($T_{2G} \propto 1/\chi(X=0)$).

3. Discussion of the results

3.1. *Single-particle properties*

3.1.1. *Theory*

Before we present results for the transport properties, we shall summarize some of the basic physics in the Hubbard model that is obtained from the dynamical mean-field theory. The Coulomb parameter U is fixed at $U = 4$. This choice may appear to be arbitrary at a first glance especially since it lies close to the Mott phase boundary, but the main effect of U (when one is off half filling and is in the strong-coupling regime) is to determine the characteristic low-energy scale [39], and $U = 4$ is a convenient choice for numerical and presentational reasons.

As the temperature is lowered, the Hubbard model in infinite d is found to always be a Fermi liquid [11, 30], except for the region of phase space where it is magnetic [40, 41]. A Fermi liquid is defined by a self-energy that has the following structure:

$$\begin{aligned} \mathrm{Re}\,[\Sigma(\omega + \mathrm{i}0^+)] &= \mathrm{Re}\,[\Sigma(0)] + \omega(1 - Z) + \mathrm{O}(\omega^2), \\ \mathrm{Im}\,[\Sigma(\omega + \mathrm{i}0^+)] &= -\Gamma + \mathrm{O}(\omega^2), \end{aligned} \tag{19}$$

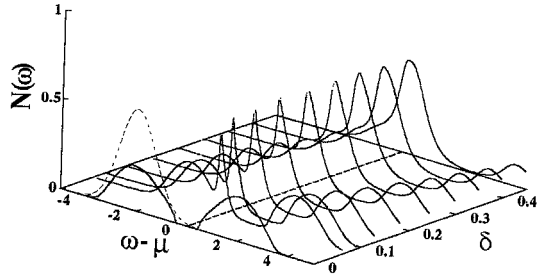

Figure 4. Single-particle DOS of the Hubbard model for different dopings $\delta = 1 - \langle n \rangle$ at an inverse temperature $\beta = 43{\cdot}2$. At half-filling ($\delta = 0$) the DOS has a gap between the lower and upper Hubbard bands. Away from half-filling a resonance occurs at the chemical potential in addition to the lower and upper Hubbard bands. This resonance becomes broader with increasing δ and finally merges with the lower Hubbard band. The broken curve at $\delta = 0$ displays the (shifted) non-interacting DOS.

with $\Gamma \propto T^2$ for temperatures $T \ll T_0$, the characteristic low-temperature scale. (The effective Fermi temperature T_0 decreases to zero as half filling is approached whenever U is larger than the critical value for the Mott transition [18], and the Fermi-liquid-theory form of equation (19) *still holds for moderate temperatures*, with the only change being that $\Gamma \propto T$ for $T > T_0$.) The spectral weight then assumes the form

$$A_{\mathbf{k}}(\omega) = \frac{1}{\pi} \frac{\Gamma}{\Gamma^2 + (\omega Z + \varepsilon_F - \varepsilon_{\mathbf{k}})^2} + A_{\mathbf{k}}^{\mathrm{Inc}}(\omega), \tag{20}$$

with the Fermi level defined by $\varepsilon_F := \mu - \mathrm{Re}\,\Sigma(0)$ and $A_{\mathbf{k}}^{\mathrm{Inc}}(\omega)$ denoting the (rather structureless) incoherent contributions to the spectral function. The spectral function includes a delta function at zero temperature ($A_{\mathbf{k}}(\omega) \to \delta(\omega Z + \varepsilon_F - \varepsilon_{\mathbf{k}}) + A_{\mathbf{k}}^{\mathrm{Inc}}(\omega)$) because the broadening Γ vanishes in that limit. The single-particle DOS $N(\omega)$ is defined to be the integral of the spectral function over all momentum:

$$N(\omega) := \sum_{\mathbf{k}} A_{\mathbf{k}}(\omega). \tag{21}$$

Figure 4 shows the evolution of the single-particle density of states as a function of doping for a fixed temperature ($\beta = 43{\cdot}2$). In addition, the (shifted) DOS for the non-interacting system has been added for comparison (broken curve at $\delta = 0$). At half-filling, the doping satisfies $\delta = 0$, and the system shows a pseudo-gap in the DOS. Very similar results are seen in iterated second-order perturbation theory [37]. Note that the lower and upper Hubbard bands centred at $\omega \approx \pm U/2$ have the same approximate width as the free DOS but are decreased by a factor of two from the unperturbed height owing to the correlations. Away from half-filling ($\delta \neq 0$), a sharp resonance appears near the chemical potential. As the doping δ increases, the width of this resonance also increases and it starts to merge with the lower Hubbard band. For dopings $\delta > 0{\cdot}4$ both low-energy peaks become indistinguishable, implying that the system has become an uncorrelated metal. The upper Hubbard band seen in figure 4 is, on the other hand, well separated from the low-energy excitations by a pseudo-gap of order U and thus contributes only to high-energy features in for example the optical conductivity [17].

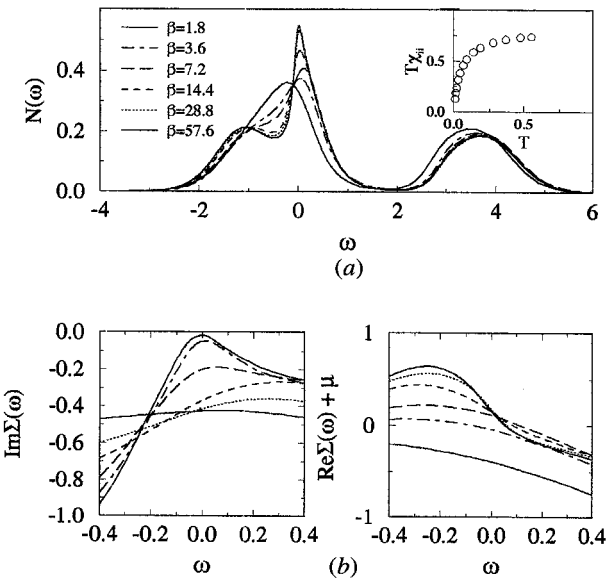

Figure 5. (*a*) The evolution of the density of states when $U = 4$ and $\delta = 0{\cdot}188$. The development of a sharp peak at the Fermi surface is correlated with the reduction of the screened local moment $T\chi_{ii}(T)$, as shown in the inset. Hence the development of the peak may be associated with a resonant Kondo screening of the spins. (*b*) The real and imaginary parts of the self-energy for various temperatures when $U = 4$ and $\delta = 0{\cdot}188$. Note that as the temperature is lowered, Im $[\Sigma(\omega)]$ becomes parabolic in ω, indicating the formation of a Fermi liquid.

Figure 5 collects the behaviour of the DOS (figure 5 (*a*)) and the real and imaginary parts of the single-particle self-energy (figure 5 (*b*)) as the temperature is reduced at fixed doping ($\delta = 0{\cdot}188$). The resonance at μ appears to be strongly temperature dependent, vanishing as T increases. For low temperatures $T \ll T_0$, the peak is centred near the chemical potential, and the height saturates to the value of the non-interacting DOS $N_0(\omega = 0) = 1/\pi^{1/2} \approx 0{\cdot}56$. The upper bound for the local DOS follows from the following simple argument (that does not require Fermi-liquid-theory behaviour). Since the self-energy is **k** independent, the interacting DOS may be written as

$$N(\omega) = \int_{-\infty}^{\infty} d\varepsilon N_0(\varepsilon) \left(-\frac{1}{\pi}\right) \mathrm{Im}\left(\frac{1}{\zeta - \varepsilon}\right), \tag{22}$$

with $\zeta := \omega - \Sigma(\omega + i0^+)$ being a complex number. Applying the mean-value theorem, we obtain

$$N(\omega) = N_0(\xi) \int_{-\infty}^{\infty} d\varepsilon \left(-\frac{1}{\pi}\right) \mathrm{Im}\left(\frac{1}{\zeta - \varepsilon}\right) = N_0(\xi) \leqslant N_0(0), \tag{23}$$

with a suitably chosen ξ. This implies that we must always have $N(\omega) \leqslant N_0(0) = 1/\pi^{1/2}$, but it *does not* tell us whether and where this maximal value will be reached (although the maximum is attained at $\omega = -\varepsilon_F/Z$ as $T \to 0$ for a Fermi liquid). Since, on the other hand, the local DOS is obtained from an effective single-impurity Anderson model, we expect strong resonant scattering at μ in the correlated limit, that is the system tends to provide a large DOS near the Fermi level. However, it cannot build up a DOS

Values of the Kondo scale T_0 for different dopings when $U = 4$.

$\delta = 1 - \langle n \rangle$	T_0
0·0680	0·0177
0·0928	0·0273
0·1358	0·0478
0·1878	0·0730
0·2455	0·1074

everywhere, but has to adjust itself in such a way that the sum rule in equation (23) is fulfilled. The system therefore satisfies a delicate self-consistent Friedel sum rule.

The development of the observed resonance as $T \rightarrow 0$ is accompanied by a strong reduction is the effective local magnetic moment $T\chi_{ii}(T)$ (see inset of figure 5 (*a*)). This simultaneous appearance of the resonance at μ and vanishing of the effective local moment suggests that this effect may be attributed to a Kondo-like quenching of the local magnetic moment in the system [18, 39]. The corresponding low-energy scale, which also sets the width of the resonance at μ seen in figures 4 and 5, may be estimated from $1/\chi_{ii}(T = 0)$ and is given in the table. Note, however, that unlike conventional Kondo systems described by Anderson's model, where one uncorrelated band couples to a localized correlated state, leading to the quenching of the latter's moments, there exists only one type of electron in the Hubbard model (1) which provides the band that is used to quench its own moments. This is a new effect which we propose to be called the 'collective single-band Kondo effect'.

We can also examine the spectra obtained from the self-energy by angle-resolved photoemission spectroscopy (ARPES). Although it is a crude approximation, we assume that the local self-energy describes the self-energy of a two-dimensional Hubbard model on a square lattice. Taking a cut along the Γ–M direction in the Brillouin zone we obtain the spectra shown in figure 6 for $U = 4$, $\beta = 43{\cdot}2$, $\langle n \rangle = 1$ (figure 6 (*a*)) and $\langle n \rangle = 0{\cdot}8122$ (figure 6 (*b*)) (note that this approximation does not distinguish between a cut along the diagonal Γ–M or along the k_x and k_y axes Γ–X–M because the self-energy is local and does not depend upon **k**). While the system is clearly insulating and not Fermi liquid like at half-filling, a typical quasiparticle peak appears when the Fermi surface is crossed away from half-filling. In addition two strongly damped bands (the lower and upper Hubbard bands) can be seen at higher energies in both figures. When the data in figure 6 (*b*) is multiplied by the Fermi function (at $\beta = 43{\cdot}2$), one arrives at the typical ARPES result in figure 7. This is quite analogous to what is seen in QMC simulations for true 2D clusters [51].

Using the peak positions in figure 6 as a definition of the quasiparticle energies $E_{\mathbf{k}}$, yields the band structure shown in figure 8. At half-filling (figure 8 (*a*)) there are two cosine-like bands below and above μ, which represent the lower and upper Hubbard bands respectively. They are separated by an indirect gap of order $U/2$. Away from half-filling, the upper and lower Hubbard bands are flattened relative to their values at half-filling (with the most flattening occurring near the Fermi level). In addition, a dynamically generated flat quasiparticle band can also be seen. This band is the flattest of the three and has a surprisingly small dispersion near the X point, which compares qualitatively with those obtained for small 2D Hubbard-clusters [51, 52], and supports the conjecture that the dynamical mean-field theory already gives an accurate picture for the single-particle properties down to $d = 2$. Note that the flatness near the X point

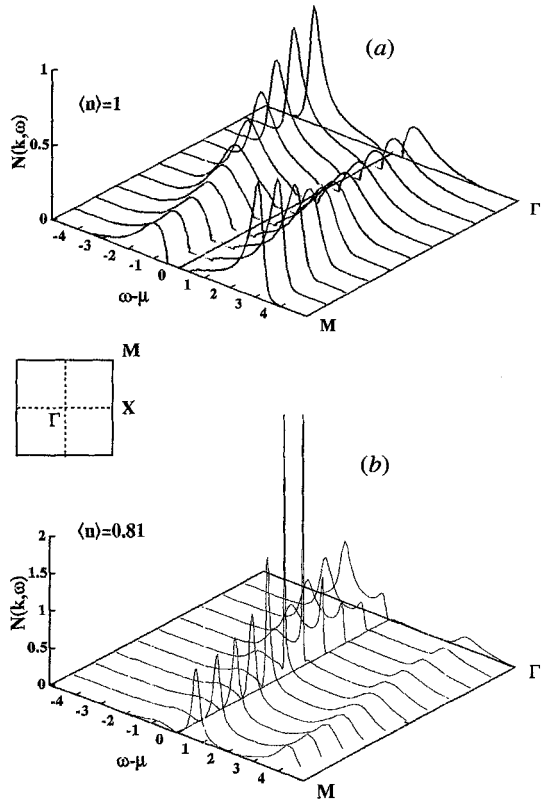

Figure 6. Angle-resolved spectra for $U = 4$, $\beta = 43{\cdot}2$ and (*a*) $\langle n \rangle = 1$ and (*b*) $\langle n \rangle = 0{\cdot}8122$ along the Γ–M direction of a 2D Brillouin zone. As expected at half-filling, the system shows a gap at μ throughout the entire zone. Away from half-filling a quasiparticle peak develops when the Fermi surface is crossed. In addition, there are strongly damped features at the position of the upper Hubbard band. The data for half-filling were obtained with the NCA.

arises from both the flatness of the non-interacting band structure, and the many-body renormalizations that reduce the quasiparticle band width.

3.1.2. *Experiment*

Only qualitative comparisons can be made between experimental photoemission spectroscopy (PES) and inverse photoemission spectroscopy (IPES) and theoretically generated spectra, because the experimental resolution broadening, the selection rules for the matrix elements, and the internal dynamics of the scattering and relaxation processes ultimately alter the experimentally measured spectrum from its theoretical counterpart. In addition (with the exception of first-principles calculations), simplified electronic models are used that are restricted to specific energy regions (mostly the low-energy regions). Nevertheless one may at least identify certain features of the model with trends found in experiments.

The spectra measured by PES and IPES of the cuprates have as their most interesting trend an increase in spectral weight close to the valence band of the insulating parent compound as the system is doped (for a review see [53]). This behaviour is completely different from what one expects in a simple rigid-band picture in which the spectrum should be insensitive to doping with only the Fermi energy changing. Obviously, a

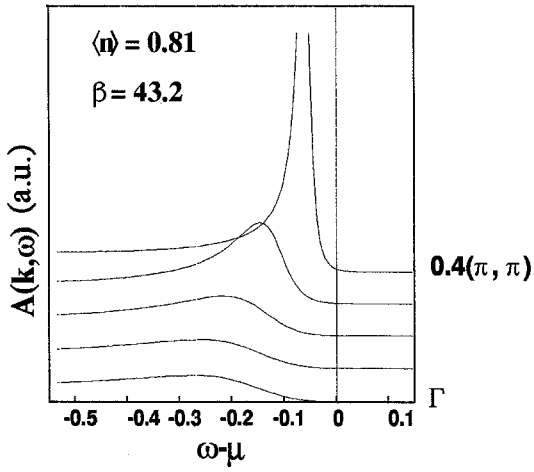

Figure 7. The data in figure 6(*b*) for Γ–M multiplied by the Fermi function (at $\beta = 43{\cdot}2$) and restricted to the low-energy part (a.u., arbitrary units). This is the type of spectrum that would typically be observed in an ARPES experiment (for example [57]). Data for **k** beyond $0{\cdot}4(\pi, \pi)$ were dropped because these features are cut off by the Fermi function.

similar trend is observed in the theoretical spectra where the quasiparticle resonance due to the collective Kondo effect develops right at the top of the lower Hubbard band as the system is doped (see figure 4).

The quasi-2D nature of the cuprates is especially appealing to the application of ARPES measurements. Accordingly the cuprates have been exhaustively studied with this technique [50, 54–57]. The general behaviour found for the low-energy portion of the ARPES results agrees with our results in that an experimental feature that might be identified with the quasiparticle peak† crosses the Fermi level in the Γ–M direction just like the theoretical result in figure 7. Assuming the low-energy excitations to be Fermi liquid like [58] produces a quasiparticle band structure that also shows flat bands near the X point of the Brillouin zone [57, 69, 60] identical with the theoretically generated quasiparticle band in figure 8. Since our results were obtained within a dynamical mean-field theory that is rather insensitive to details of the underlying lattice structure, the agreement between experiment and theory is strong evidence that the low-energy single-particle dynamics are produced by strong electronic correlations independent of the dimensionality!

3.2. *Optical conductivity*

3.2.1. *Theory*

The optical conductivity $\sigma(\omega)$ is another important probe of a strongly correlated system. It measures the rate at which electron–hole pairs are created by photons of frequency ω. Figure 9 shows the results [61] for $\sigma(\omega)$ obtained from equation (5) when $\delta = 0{\cdot}068$ for a variety of temperatures (figure 9 (*a*)) and results for $\beta = 43{\cdot}2$ and various dopings δ (figure 9 (*b*)). The Drude peak at $\omega = 0$ develops with decreasing temperature. In addition there appears a small midinfrared peak at $\omega \approx 1$. As shown in figure 9 (*b*),

† The assumption of this peak being Fermi liquid like is still heavily discussed (for example [50, 58]).

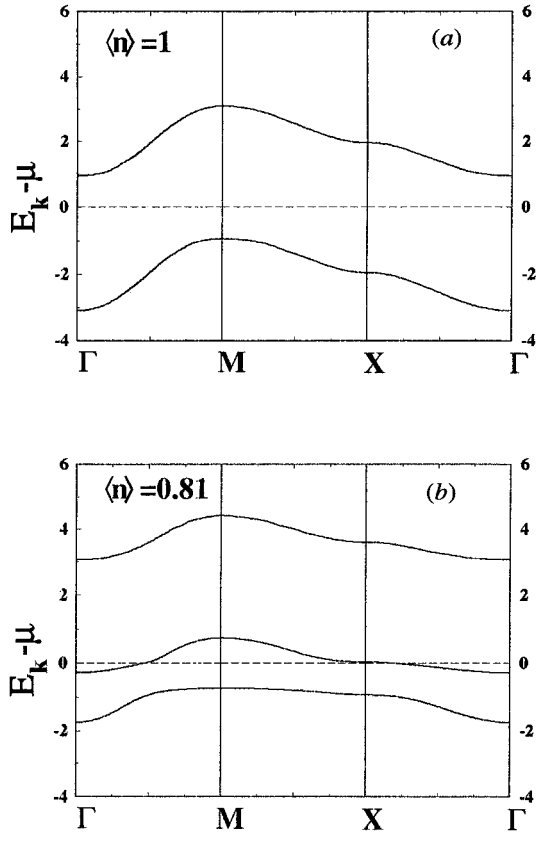

Figure 8. Band structure for the Hubbard model obtained from the self-energy in figure 6.

this peak is more pronounced for small δ but remains visible even at larger doping. In addition, it is strongly temperature dependent and clearly visible only for the lowest temperatures. We attribute it to excitations from the lower Hubbard band to the quasiparticle band at the chemical potential. The last feature in $\sigma(\omega)$ is a roughly temperature-independent peak at $\omega \approx U$ owing to the charge excitations from the lower part of the spectrum, that is from the lower Hubbard band and the quasiparticle peak at μ, to the upper Hubbard band (cf. figure 5).

The insets of figure 9 show the development of the Drude weight as obtained from equation (7) as a function of doping (figure 9 (*b*)) and the width of the Drude peak as function of temperature (figure 9 (*a*)). The latter was obtained by fitting the generic form

$$\sigma(\omega \to 0) = \frac{D}{\pi} \frac{\tau}{1 + \tau^2 \omega^2} \tag{24}$$

to the low-frequency regions in figure 9 (*a*). The Drude weight initially increases linearly with δ and then saturates to its maximal value at $\delta \approx 0{\cdot}5$, before decreasing. This behaviour can be understood in terms of a simple picture. The Drude weight is determined by the carrier density and effective mass via $D \propto n/m^*$. From the doping dependence of the quasiparticle peak in the spectra in figure 4, one may assume that $m^{*-1} \propto \delta$. The carrier density, on the other hand, is given by $n \approx 1 - \delta$, that is $D \propto \delta(1 - \delta)$. This expression explains the behaviour for small doping as well as the

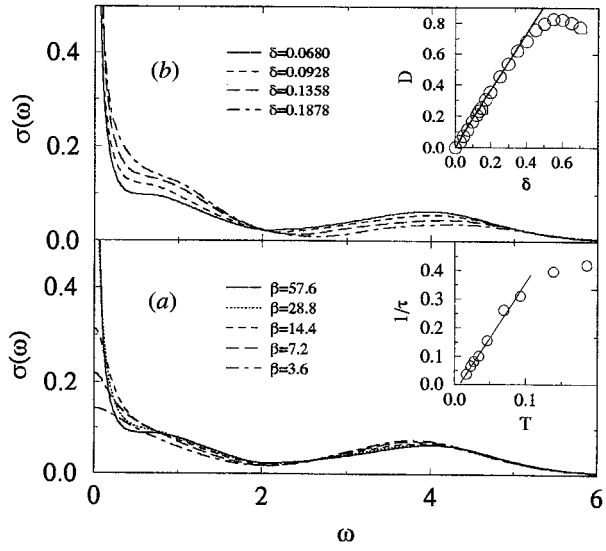

Figure 9. (*a*) Optical conductivity against ω for various temperatures when $\delta = 0{\cdot}068$. Note that at low temperatures, when the Kondo peak becomes pronounced in the DOS, a midinfrared feature begins to appear in $\sigma(\omega)$. As shown in the inset, if we fit these data to a Drude form, then the width of the Drude peak is found to increase roughly linearly with T. (*b*) Filling dependence of the optical conductivity when $U = 4$ and $\beta = 43{\cdot}2$. Note that for larger δ the midinfrared and Drude peaks begin to merge, so that the latter is less distinct. The inset shows the evolution of the Drude weight D as a function of doping. D is determined by the extrapolation method of [44].

maximum, which should lie at $\delta_{\max} \approx 0{\cdot}5$, and explains how the character of the carriers changes from being hole like near half-filling to being electron like at low densities.

The width $1/\tau$ of the Drude peak displays a linear behaviour $1/\tau \sim T$ for $T \lesssim 0{\cdot}1$. This dependence may be traced back to the development of the Kondo peak below T_0. Note that the intercept of the linear region does not lead to $1/\tau \to 0$ as $T \to 0$ as required, implying that for very low temperatures the Drude width decreases more rapidly ($1/\tau \sim T^2$), as expected for a Fermi liquid.

3.2.2. *Experiment*

When one tries to make contact with experiment, care has to be taken about the energy scales. The single-band Hubbard model should only be used to describe low-energy features of the cuprates [63]. It does not make sense to use our results beyond $\omega \approx 2$ in a comparison with experimental data because the higher-energy bands, corresponding to the charge-transfer insulating behaviour of the parent compounds, have been neglected in the mapping to a single-band Hubbard model.

Two types of experiment have been performed to determine the optical conductivity of the cuprates: a Kramers–Kronig analysis was employed to extract $\sigma(\omega)$ from reflectivity measurements [4, 5, 63–65]; photoinduced absorption has also been used [67, 68]. These experiments yield five low-energy trends.

(1) The midinfrared peak maximum moves to lower frequency and merges with the Drude peak as the doping increases; its spectral weight grows very rapidly with doping.

(2) At a fixed value of doping, spectral weight rapidly moves to lower ω as $T \to 0$, but the total weight in the Drude plus midinfrared peaks remains approximately constant; the width of the Drude peak decreases linearly with T.
(3) The insulating phase has a charge-transfer gap; upon doping, the optical conductivity initially increases within the gap region.
(4) There is an isosbestic point, or nearly isosbestic behaviour (in the sense that the optical conductivity is independent of doping) at a frequency that is approximately half the charge-transfer gap.
(5) More than one peak is observed in the midinfrared region.

Most of these trends are observed in the theoretical model; the midinfrared peak is observed to move to lower frequency and merge with the Drude peak as a function of doping, the optical conductivity rapidly increases within the gap region as the system is doped, and there is an isosbestic point at a frequency $\omega \approx 2$. In addition, spectral weight is transferred to lower frequencies as the temperature is decreased, and the Drude width depends linearly on the temperature for a wide range of T, but the total Drude plus midinfrared spectral weight increases as $T \to 0$. The theoretical model also does not display multiple midinfrared peaks.

These experimental features in the optical conductivity are usually attributed to either phonons or impurities but, judging from our results, the low-energy feature may also be due to excitations from the lower Hubbard band to a dynamically generated quasiparticle band at the chemical potential, that is connected to local or short-range spin fluctuations similar to those responsible for transport anomalies in the infinite-dimensional periodic Anderson model [43]. Let us stress, however, that we do not want to make the point that one is able to explain the normal state of the cuprates in all respects *quantitatively* by studying the single-band Hubbard model in the dynamical mean-field theory. We do think that our calculations display the underlying physics that drives the anomalous features found in the normal state of the cuprates, and they determine the order of magnitude of the corresponding temperature scale.

3.3. *Transport coefficients*

3.3.1. *Theory*

The creation of a dynamical low-energy scale, such as the Kondo temperature observed in the Hubbard model above, is known to be accompanied by interesting and anomalous features in transport coefficients. In our previous studies we already described the resistivity and NMR relaxation rate as striking examples for this behaviour. Figure 10 summarizes these results. Most prominent is the pronounced linear region in $\rho(T)$ which increases with increased doping. The slope of this region is proportional to $1/\delta$ as shown in the inset in figure 10 (*a*). The thermal conductivity κ was also calculated; however it is not plotted, since to a very good approximation, it follows the Wiedemann–Franz law $\kappa \propto T/\rho$. Figure 10 (*b*) presents the results for the NMR relaxation rate $1/T_1$. Here, too, a rather anomalous variation with both temperature and doping is found. A linear region in $1/T_1$ develops as the doping increases, and the slope changes sign for $\delta \approx 0{\cdot}15$. The doping dependence of $1/T_1$ is reduced as the temperature increases but does not disappear at the temperatures that can be reached by the numerical analytic continuation.

It has been recently argued that the constancy of the ratio T_1T/T_{2G} is a test for the quantum critical region of the 2D Heisenberg spins in the Cu–O planes of the cuprates [68] (even though this theory neglects the charge degrees of freedom, assuming that

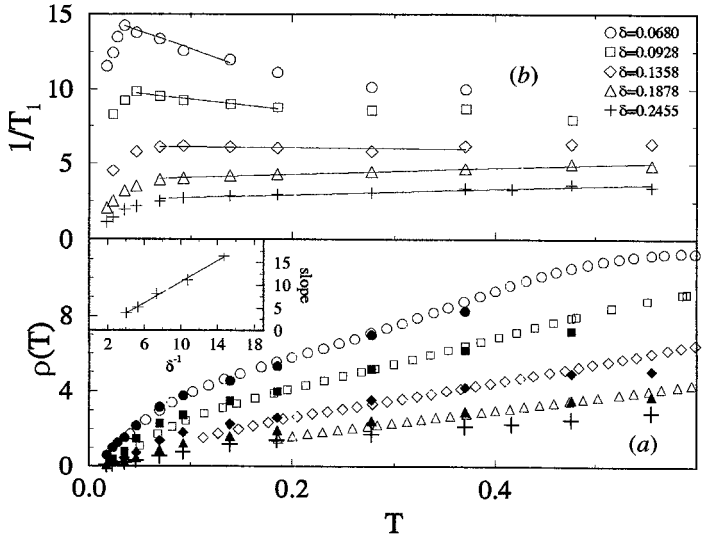

Figure 10. (*a*) Resistivity against temperature for several different dopings when $U = 4$. The open (filled) symbols are for NCA (QMC) results. There is essentially exact agreement between the NCA and QMC data for high temperatures. The slope in the linear regime, determined by a linear least-squares fit, increases linearly with $1/\delta$ as shown in the inset. The units on the vertical axis are approximately $10^3\,\Omega$cm. (*b*) NMR relaxation rate $1/T_1$ against temperature for different dopings at $U = 4t^*$. The lines are linear fits in the anomalous region.

the most important effect of the holes is to add *disorder* into the spin system). However, as seen in figure 11, this ratio also becomes flat at intermediate temperatures within the dynamical mean-field theory in infinite dimensions. The constant value of the ratio T_1T/T_{2G} increases with increasing doping but does not change significantly for the lowest values of the doping.

Finally we want to report calculations of two other interesting transport coefficients, namely the thermopower S and the Hall coefficient R_H. The strange behaviour of the

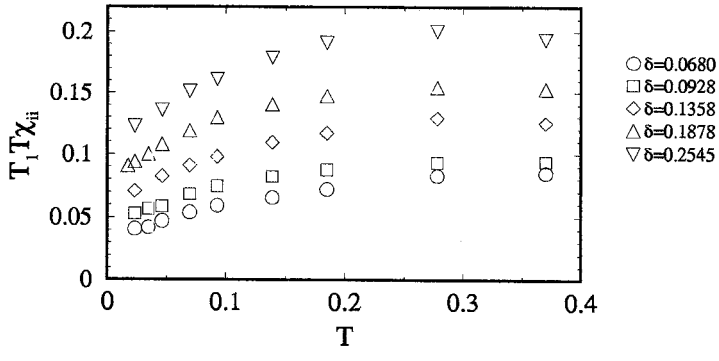

Figure 11. Ratio of the longitudinal (T_1) to transverse ($T_{2g} \propto 1/\chi_{loc}$) NMR relaxation rates multiplied by T. Note how this ratio becomes flat at intermediate values of T, which is supposed to be a signal for the quantum critical regime. The constant value of this ratio increases with increasing doping but is nearly constant near half-filling.

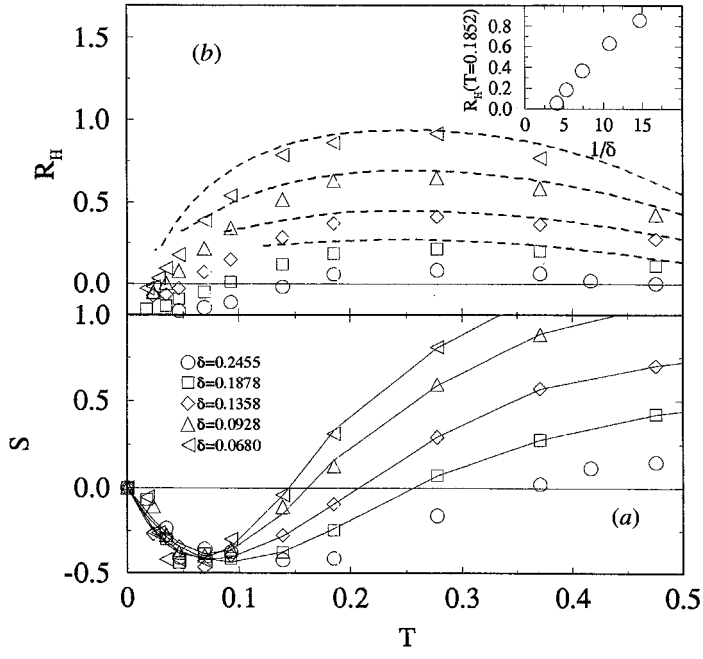

Figure 12. (*a*) Thermopower and (*b*) Hall coefficient for four different dopings δ as functions of temperature. In (*b*), the open symbols (broken curves) are QMC (NCA) results and in (*a*) the solid curves come from a fit to the QMC data (open symbols). In the inset of (*a*), the Hall coefficient $R_H(T = 0{\cdot}1852)$ at a fixed temperature is plotted against $1/\delta$, indicating that $R_H(T = 0{\cdot}1852)$ increases roughly in proportion to $1/\delta$, consistent with experimental results for the cuprates [70]. The units on the vertical axis are approximately 86 $\mu V\,K^{-1}$ for the thermopower in (*a*) and $10^{-9}m^3\,C^{-1}$ for R_H in (*b*).

latter gave rise to a number of speculations about different scattering mechanisms for transport with and without a magnetic field [69] and it is thus interesting to look at the behaviour of this quantity within our scheme. Figure 12 compiles the results for S (figure 12(*a*)) and R_H (figure 12(*b*)) for four different dopings as functions of temperature. The thermopower shows the sign change at intermediate temperatures that is characteristic of correlated materials. The Hall coefficient, in figure 12(*b*), is more interesting. It is positive for high temperatures and displays a maximum at intermediate temperatures, followed by a strong decrease for lower T, eventually becoming negative (qualitatively similar features have been seen in simulations of the 2D Hubbard model [71]). Interestingly, the position of the maximum is weakly sensitive to doping while, as shown in the inset, its height roughly decreases with increasing doping like $R_H \sim 1/\delta$. Finally, we show the quadratic behaviour of the Hall angle ($\cot\Theta_H = \rho_{xx}/\rho_{xy} = 1/\mu$, where μ is the charge carrier's mobility). The Hall angle is calculated with the NCA so that a dense set of points may be presented at high temperatures, where the analytical continuation of QMC data becomes numerically expensive. Here the agreement between the NCA and the QMC data is essentially exact (cf. figure 12). Figure 13 plots the inverse mobility as function of temperature for two dopings (cf. figure 1 for typical experimental temperature and doping dependence in the cuprates). The Hall angle is plotted as a function of T^2 in the inset of figure 13. It shows a roughly linear behaviour on this scale.

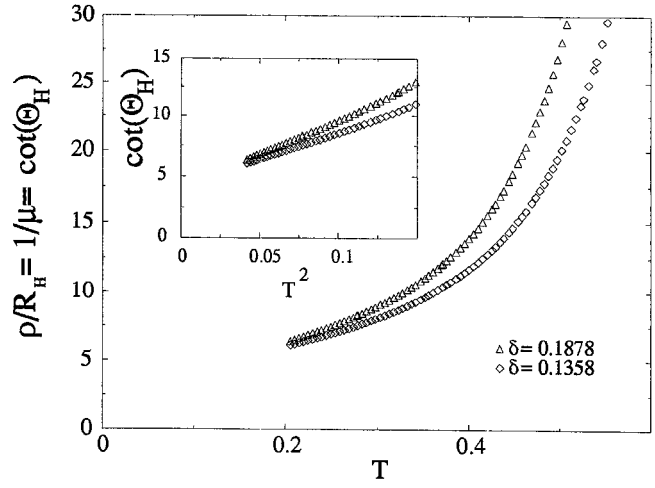

Figure 13. Inverse mobility $1/\mu = \rho/R_H = \cot\Theta_H$ calculated with the NCA for two dopings as function of T for large T. The NCA was used since it is essentially exact at these temperatures (cf. figure 12), and significantly less computationally expensive, thus allowing us to present a dense data set. In the inset the Hall angle $\cot\Theta_H$ is plotted as a function of T^2. Note the apparent linear behaviour.

3.3.2. *Experiment*

As we have pointed out [18], the theoretical behaviour is consistent with the normal-state properties of hole-doped high-T_c compounds. As is well known, the experimental trends observed include the following [2, 70] (cf. also figure 1).

(1) A (sub)linear variation in the resistivity occurs with temperature, the slope or absolute value of $\rho(T)$ for a given T decreasing with $1/\rho$.
(2) The NMR rate drops with increasing doping owing to a decrease in the (local) spin fluctuations and shows a linear tail with positive slope at intermediate temperatures; there is also a tendency towards a change in sign of the slope of this linear region with decreasing doping.
(3) The spin–lattice relaxation rate T_1 becomes doping independent at intermediate values of the temperature, and the ratio T_1T/T_{2G} becomes constant over a similar temperature range.
(4) The Hall coefficient goes through a maximum whose position is roughly independent of doping but whose height decreases proportional to $1/\rho$.
(5) The Hall angle $\cot\Theta_H$ is usually found to vary like T^2 over a considerable temperature range.

Since all these features (except the constancy of $1/T_1$ with respect to doping at intermediate T) are consistently obtained from the dynamical mean-field theory, including the peculiar behaviour of the Hall angle (without any necessity to resort to an exotic ground-state or scattering mechanism) and the constancy of the ratio T_1T/T_{2G}, we anticipate that these anomalies are intrinsic properties of strong local correlations and do not specifically depend on the low dimensionality of the cuprates. This statement is further supported by the observation that similar features in the NMR and electron paramagnetic resonance relaxation rates and the Hall coefficient are also found in 'conventional' heavy-fermion materials [16, 72].

4. Summary and conclusion

We presented results for a variety of transport properties that support the conjecture that most of the anomalous normal-state properties of the high-T_c compounds are intrinsic properties resulting from correlation effects in a single-band model. These anomalies include a resistivity linear in T and anomalies in the temperature dependence of the NMR relaxation rate and thermopower. We also presented a method to calculate the Hall conductivity and Hall coefficient that does not rely on the (conventionally used) relaxation-time approximation or the introduction of a new scattering mechanism such as Coleman's 'skew scattering'. This new method enabled us to obtain physically sensible results for the Hall coefficient, showing a positive sign and a temperature dependence characteristic of strongly correlated systems. We also found that the Hall angle or inverse mobility of the carriers shows a clear T^2 behaviour as also observed in the cuprates. The optical conductivity was found to have a Drude peak at small ω, a charge excitation peak at $\omega \approx U$, and a midinfrared feature that is attributed to excitations from the lower Hubbard band to the quasiparticle band dynamically generated at the Fermi level.

Most of these properties also show a distinctive dependence upon doping. The Drude weight increases linearly with increasing doping δ and both the slope of the linear region in the resistivity and the Hall coefficient increase as $1/\delta$. The midinfrared feature in the optical conductivity initially increases rapidly with doping and then decreases as δ increases further (but is still visible up to $\delta \approx 0{\cdot}20$).

These features are also found in the high-T_c materials and to some extent in heavy-fermion or mixed-valence compounds. From our results it seems that the appearance and overall temperature dependence of these anomalies is due to the existence of strong local correlations that lead to a dynamically generated (strongly temperature-dependent) low-energy scale arising from a Kondo-like screening of the (local) magnetic moments. The anomalous regions are more pronounced in the present case, which may be attributed to the fact that in the Hubbard model only one band exists, that is the electrons that form the moments are also responsible for their screening, while these different tasks are split between at least two bands in the periodic Anderson model. To distinguish between these different physical situations we suggest that the singlet formation found in the Hubbard model should be labelled as a collective 'single-band Kondo effect'.

Motivated by these considerations, we propose that the peculiar anomalies found in the cuprates may be viewed as a cross-over phenomenon from a high-temperature 'normal' phase to a renormalized Fermi liquid as $T \to 0$. The anomalous temperature dependence of physical quantities is then obtained from the peculiar T behaviour of the developing quasiparticle band at μ. Note that, in several heavy-fermion compounds, true Fermi-liquid behaviour is not observed, because the development of the Fermi liquid is pre-empted by a phase transition into an ordered state. It was fortuitous that the first heavy-fermion compounds studied did have transition temperatures much smaller than T_K, enabling one to observe the formation of the heavy Fermi liquid first. In the cuprates, on the other hand, it may be that the relevant Kondo scale is of the same order as the transition temperatures, and we are in a situation where the mentioned cross-over is observed, but that the system undergoes a phase transition before a Fermi liquid forms [73].

Acknowledgments

We would like to acknowledge useful conversations with F. F. Assaad, W. Chung, J. Keller, Y. Kim, C. Quitmann, D. Scalapino, R. Scalettar, R. Singh, D. Tanner, and

G. Thomas. This work was supported by the National Science Foundation (NSF) under grant DMR-9406678, the NATO Collaborative Research Grant CRG 931429 and through the NSF NYI program under grant DMR-9357199. In addition, we would like to thank the Ohio Supercomputing Center, and the Physics department of the Ohio State University for providing computer facilities.

References

[1] BEDNORZ, J. G., and MÜLLER, K. A., 1986, *Z. Phys.*, **64,** 189.
[2] PENNINGTON, C. H., and SLICHTER, C. P., 1989, *Physical Properties of High Temperature superconductors*, Vol. 2, edited by D. M. Ginsberg (Singapore: World Scientific); ONG, N. P., and IYE, Y., 1989, *Physical Properties of High Temperature Superconductors*, Vol. 3, edited by D. M. Ginsberg (Singapore: World Scientific).
[3] QUITMANN, C., Ph.D. Thesis, Aachen, 1992.
[4] TIMUSK, T., and TANNER, D. B., 1989, *Physical Properties of High Temperature Superconductors*, Vol. 1, edited by D. M. Ginsberg (Singapore: World Scientific), pp. 339–407.
[5] RENK, K. I., 1994, *Tl-Based High Temperature Superconductors*, edited by A. M. Hermare and J. V. Yakhmi (New York: Marcel Dekker), pp. 447–510.
[6] ANDERSON, P. W., 1987, *Frontiers and Borderlines in Many Particle Physics*, Proceedings of the International School of Physics 'Enrico Fermi' (Amsterdam: North-Holland), p. 1. ANDERSON, P. W., 1987, *Science*, **235,** 1196.
[7] BASKARAN, G., and ANDERSON, P. W., 1988, *Phys. Rev.* B, **37,** 850.
[8] SÓLYOM, J., 1979, *Adv. Phys.*, **28,** 201.
[9] ANDERSON, P. W., 1991, *Physica* C, **185,** 11.
[10] VARMA, C. M., LITTLEWOOD, P. B., SCHMITT-RINK, S., ABRAHAMS, E., and RUCKENSTEIN, A. E., 1989, *Phys. Rev. Lett.*, **63,** 1996.
[11] LEE, P., and NAGAOSA, N., 1990, *Phys. Rev. Lett.*, **64,** 2450; 1991, *Phys. Rev.* B, **43,** 1233.
[12] RUCKENSTEIN, A. E., and VARMA, C. M., 1991, *Physica* C, **185,** 134.
[13] OGATA, M., and SHIBA, H., 1990, *Phys. Rev.* B, **41,** 2326.
[14] CASTELLANI, C., DI CASTRO, C., and METZNER, W., 1994, *Phys. Rev. Lett.*, **72,** 316.
[15] STICHT, J., D'AMBRUMENIL, N., and KÜBLER, J., 1986, *Z. Phys.* B, **65,** 149.
[16] GREWE, N., and STEGLICH, F., 1991, *Reports on Physics and Chemistry of Rare Earths*, Vol. 14, p. 343.
[17] PRUSCHKE, TH., COX, D. L., and JARRELL, M., 1993, *Phys. Rev.*, **47,** 3553; 1993, *Europhys. Lett.*, **21,** 593.
[18] JARRELL, M., and PRUSCHKE, TH., 1993, *Phys. Rev.* B, **49,** 1458. PRUSCHKE, TH., and JARRELL, M., 1994, *Physica* B, **199–200,** 217.
[19] VOLLHARDT, D., 1993, *Correlated Electron Systems*, edited by V. J. Emery (Singapore: World Scientific).
[20] HUBBARD, J., 1963, *Proc. R. Soc.* A, **276,** 238. GUTZWILLER, M. C., 1963, *Phys. Rev. Lett.*, **10,** 159. KANAMORI, J., 1963, *Prog. theor. Phys, Osaka*, **30,** 257.
[21] PRUSCHKE, TH., 1990, *Z. Phys.* B, **81,** 319.
[22] DAGOTTO, E., 1991, *Int. J. mod. Phys.* B, **5,** 77; 1994, *Rev. mod. Phys.*, **66,** 1990.
[23] HIRSCH, J. E., 1987, *Phys. Rev.* B, **35,** 1851. SCALETTAR, R. T., *et al.*, 1989, *Phys. Rev.* B, **39,** 4711.
[24] METZNER, W., and VOLLHARDT, D., 1989, *Phys. Rev. Lett.*, **62,** 324.
[25] MÜLLER-HARTMANN, E., 1989, *Z. Phys.* B, **74,** 507.
[26] BRANDT, U., and MIELSCH, C., 1989, *Z. Phys.* B, **75,** 365; 1990, *Ibid.*, **79,** 295; 1991, *Ibid.*, **82,** 37.
[27] JANIŠ, V., 1991, *Z. Phys.* B, **83,** 227.
[28] KIM, C., KURAMOTO, Y., and KASUYA, T., 1990, *J. phys. Soc. Japan*, **59,** 2414.
[29] JANIŠ, V., and VOLLHARDT, D., 1992, *Int. J. mod. Phys.* B, **6,** 713.
[30] JARRELL, M., 1992, *Phys. Rev. Lett.*, **69,** 168.
[31] GEORGES, A., and KOTLIAR, G., 1992, *Phys. Rev.* B, **45,** 6479.
[32] ITZYKSON, C., and DROUFFE, J. M., 1989, *Statistical Field Theory*, Vol. I and Vol. II (Cambridge University Press).

[33] MIGDAL, A. B., 1958, *Zh. éksp. teor. Fiz.*, **34,** 1438 (Engl. Transl., 1958, *Soviet Phys. JETP*, **7,** 999). ELIASHBERG, G. M., 1960, *Zh. éksp. teor. Fiz.*, **38,** 966 (Engl. Transl., 1960, *Soviet Phys. JETP*, **11,** 696.
[34] HIRSCH, J. E., and FYE, R. M., 1986, *Phys. Rev. Lett.*, **56,** 2521.
[35] JARRELL, M., AKHLAGHPOUR, H., and PRUSCHKE, T., 1993, *Quantum Monte Carlo Methods in Condensed Matter Physics*, edited by M. Suzuki (Singapore: World Scientific).
[36] KEITER, H., and KIMBALL, J. C.,1971, *Int. J. Magn.*, **1,** 233. BICKERS, N. E., COX, D. L., and WILKINS, J. W., 1987, *Phys. Rev.* B, **36,** 2036. PRUSCHKE, TH., and GREWE, N., 1989, *Z. Phys.* B, **74,** 439.
[37] GEORGES, A., KOTLIAR, G., and SI, Q., 1992, *Int. J. mod. Phys.* B, **6,** 705. ZHANG, X. Y., ROZENBERG, M. J., and KOTLIAR, G., 1993, *Phys. Rev. Lett.*, **70,** 1666. ROZENBERG, M. J., KOTLIAR, G., and ZHANG, X. Y., 1994, *Phys. Rev.* B, **49,** 10 181. FREERICKS, J. K., and JARRELL, M., 1994, *Phys. Rev.* B, **50,** 6939.
[38] ZLATIĆ, V., and HORVATIĆ, B., 1983, *Phys. Rev.* B, **28,** 6904. HORVATIĆ, B., and ZLATIĆ, V., 1985, *J. Phys., Paris*, **46,** 1459. ZLATIĆ, V., HORVATIĆ, B., and SOKCEVIC, D., 1985, *Z. Phys.* B, **59,** 151. HORVATIĆ, B., SOKCEVIC, D., and ZLATIĆ, V., 1987, *Phys. Rev.* B, **36,** 675.
[39] JARRELL, M., and PRUSCHKE, TH., 1993, *Z. Phys.* B, **90,** 187.
[40] FREERICKS, J. K., and JARRELL, M., 1995, *Phys. Rev. Lett.*, **74,** 186.
[41] VAN DONGEN, P. G. J., 1991, *Phys. Rev. Lett.*, **67,** 757; 1995, *Phys. Rev. Lett.*, **74,** 182.
[42] KHURANA, A., 1990, *Phys. Rev. Lett.*, **64,** 1990.
[43] SCHWEITZER, H., and CZYCHOLL, G., 1990, *Z. Phys.* B, **77,** 327; 1991, *Phys. Rev. Lett.*, **67,** 3724.
[44] SCALAPINO, D. J., WHITE, S., and ZHANG, S., 1993, *Phys. Rev.* B, **47,** 7995.
[45] MADELUNG, O., 1978, *Introduction to Solid-State Theory* (Berlin: Springer).
[46] COLEMAN, P., ANDERSON, P. W., and RAMAKRISHNAN, T. V., 1985, *Phys. Rev. Lett.*, **55,** 414.
[47] VORUGANTI, P., GOLUBENTSEV, A., and JOHN, S., 1992, *Phys. Rev.* B, **45,** 13 945.
[48] PENNINGTON, C., and SLICHTER, C. P., 1991, *Phys. Rev. Lett.*, **66,** 381.
[49] THELEN, D., and PINES, D., 1994, *Phys. Rev.* B, **49,** 3528.
[50] OLSON, C. G., LIU, R., LYNCH, D. W., LIST, R. S., ARKO, A. J., VEAL, B. W., CHANG, Y. C., JIANG, P. Z., and PAULIKAS, A. P., 1990, *Phys. Rev.* B, **42,** 381.
[51] BULUT, N., SCALAPINO, D. J., and WHITE, S. R., 1994, *Phys. Rev.* B, **50,** 7215.
[52] HANKE, W., *et al.*, 1995, unpublished.
[53] ALLEN, J. W., 1991, *Physica* B, **171,** 175; ALLEN, J. W., *et al.*, 1992, *Int. J. mod. Phys.* G, **546,** 453.
[54] CAMPUZANO, J. C., *et al.*, 1990, *Phys. Rev. Lett.*, **64,** 2308. CAMPUZANO, J. C., SMEDSKJAER, L. C., BENEDEK, R., JENNINGS, G., and BANSIL, A., 1991, *Phys. Rev.* B, **43,** 2788.
[55] LIU, R., VEAL, B. W., PAULIKAS, A. P., DOWNEY, J. W., SHI, H., OLSON, C. G., GU, C., ARKO, A. J., and JOYCE, J. J., 1992, *Phys. Rev.* B, **45,** 5614. LIU, R., *et al.*, 1992, *Phys. Rev.* B, **46,** 11 056.
[56] KING, D. M., *et al.*, 1993, *Phys. Rev. Lett.*, **70,** 3159.
[57] DESSAU, D., 1992, Ph.D. Thesis, Stanford University. DESSAU, D., *et al.*, 1993, *Phys. Rev. Lett.*, **71,** 2781.
[58] LIU, L. Z., ANDERSON, R. O., and ALLEN, J. W., 1991, *Proceedings of Workshop on Fermiology of High T_c*, Argonne National Laboratory, 25–27 March 1991.
[59] ABRIKOSOV, A. A., CAMPUZANO, J. C., and GOFRON, K., 1993, *Physica* C2, **14,** 73.
[60] GOFRON, K. J., CAMPUZANO, J. C., DING, H., GU, C., LIU, R., DABROWSKI, B., VEAL, B. W., CRAMER, W., and JENNINGS, G., 1993, *J. Phys. Chem. Solids*, **54,** 1193.
[61] JARRELL, M., FREERICKS, J. K., and PRUSCHKE, TH., 1995, *Phys. Rev.* B, **51,** 11 704.
[62] ZHANG, F. C., and RICE, T. M., 1988, *Phys. Rev.* B, **37,** 3759.
[63] ORENSTEIN, J., THOMAS, G. A., MILLIS, A. J., COOPER, S. L., RAPKINE, D. H., TIMUSK, T., SCHNEEMEYER, L. F., and WASZCZAK, J. V., 1990, *Phys. Rev.* B, **42,** 6342. THOMAS, G. A., RAPKINE, D. H., COOPER, S. L., CHEONG, S.-W., and COOPER, A. S., 1991, *Phys. Rev. Lett.*, **67,** 2906. THOMAS, G. A., RAPKINE, D. H., COOPER, S. L., CHEONG, S.-W., COOPER, A. S., SCHNEEMEYER, L. F., and WASZCZAK, J. V., 1992, *Phys. Rev.* B, **45,** 2474. THOMAS, G. A., 1991, *Proceedings from the 39th Scottish Universities Summer School in Physics*, edited by D. P. Tunstall, W. Barford and P. Osborne (New York: Adam Hilger).

[64] UCHIDA, S., IDO, T., TAKAGI, H., ARIMA, T., TOKURA, Y., and TAJIMA, S., 1991, *Phys. Rev.* B, **43,** 7942. UCHIDA, S., 1992, *J. Phys. Chem. Solids*, **53,** 1603. UCHIDA, S., TAKAGI, H., TOKURA, Y., KOSHIHARA, S., and ARIMA, T., 1989, *Strong Correlation and Superconductivity*, edited by H. Fukuyama, S. Maekawa and A. P. Malozemoff (Tokyo: Springer), pp. 194–203.

[65] ROMERO, D. B., PORTER, C. D., TANNER, D. B., FORRO, L., MANDRUS, D., MIHALY, L., CARR, G. L., and WILLIAMS, G. P., 1992, *Phys. Rev. Lett.*, **68,** 1590. FORRO, L., CARR, G. L., WILLIAMS, G. P., MANDRUS, D., and MIHALY, L., 1990, *Phys. Rev. Lett.*, **65,** 1941.

[66] YU, G., LEE, C. H., MIHAILOVIC, D., HEEGER, A. J., FINCHER, C., HERRON, N., and MCCARRON, E. M., 1993, *Phys. Rev.* B, **48,** 7545.

[67] KIM, Y. H., CHEONG, S.-W., and FISK, Z., 1991, *Phys. Rev. Lett.*, **67,** 2227.

[68] IMAI, T., SLICHTER, C. P., YOSHIMURA, K., KATOH, M., and KOSUGE, K., 1993, *Phys. Rev. Lett.*, **71,** 1254. SOKOL, A., and PINES, D., 1993, *Phys. Rev. Lett.*, **71,** 2813. CHUBUKOV, A. V., SACHDEV, S., and SOKOL, A., 1994, *Phys. Rev.* B, **49,** 9052. CHUBUKOV, A. V., SACHDEV, S., and YE, J., 1994, *Phys. Rev.* B, **49,** 11 919.

[69] ANDERSON, P. W., 1991, *Phys. Rev. Lett.*, **67,** 2092.

[70] ONG, N. P., WANG, Z. Z., CLAYHOLD, J., TARASCIN, J. M., GREENE, L. H., and MCKINNON, W. R., 1987, *Phys. Rev.* B, **35,** 8807; TAKAGI, H., IDO, T., ISHIBASHI, S., UOTU, M., UCHIDA, S., and TOKURA, Y., 1989, *Phys. Rev.*. B, **40,** 225.

[71] ASSAAD, F. F., and IMADA, M., 1995, *Phys. Rev. Lett.*, **74,** 3872.

[72] LOIDL, A., 1995, private communication.

[73] LEVIN, K., KIM, J. H., LU, J. P., and SI, Q., 1991, *Physica* C, **175,** 449.